COMPARISON OF THE PERFORMANCE OF DIFFERENT TIME DELAY ESTIMATION TECHNIQUES FOR ULTRASOUND ELASTOGRAPHY

A Thesis

by

SRINATH SAMBASUBRAMANIAN

Submitted to the Office of Graduate Studies of
Texas A&M University
in partial fulfillment of the requirements for the degree of

MASTER OF SCIENCE

August 2010

Major Subject: Electrical Engineering

COMPARISON OF THE PERFORMANCE OF DIFFERENT TIME DELAY ESTIMATION TECHNIQUES FOR ULTRASOUND ELASTOGRAPHY

A Thesis

by

SRINATH SAMBASUBRAMANIAN

Submitted to the Office of Graduate Studies of
Texas A&M University
in partial fulfillment of the requirements for the degree of

MASTER OF SCIENCE

Approved by:

Chair of Committee,	Raffaella Righetti
Committee Members,	Jim Ji
	Deepa Kundur
	Javier Jo
Head of Department,	Costas Georghiades

August 2010

Major Subject: Electrical Engineering

ABSTRACT

Comparison of the Performance of Different Time Delay Estimation Techniques for Ultrasound Elastography. (August 2010)

Srinath Sambasubramanian, B.Tech. , National Institute of Technology, Tiruchirapalli

Chair of Advisory Committee: Dr. Raffaella Righetti

Elastography is a non-invasive medical imaging modality that is used as a diagnostic tool for the early detection of several pathological changes in soft tissues. Elastography techniques provide the local strain distributions experienced by soft tissues due to compression. The resulting strain images are called “elastograms”. In elastography, the local tissue strains are usually estimated as the gradient of local tissue displacement. The local tissue displacements are estimated from the time delays between gated pre- and post-compression echo signals. The quality of the resulting elastograms is highly dependent on the accuracy of these local displacement estimates. While several time delay estimation (TDE) techniques have been proposed for elastography applications, there is a lack of systematic study that statistically compares the performance of these techniques. This information could prove to be of great importance to improve currently employed elastographic clinical methods.

This study investigates the performance of selected time delay estimators for elastography applications. Time delay estimators based on Generalized Cross Correlation (GCC), Sum of Squared Differences (SSD) and Sum of Absolute

Differences (SAD) are proposed and implemented. Within the class of GCC algorithms, we further consider: an FFT-based cross correlation algorithm (GCC-FFT), a hybrid time-domain and frequency domain cross correlation algorithm with prior estimates (GCC-PE) and an algorithm based on the use of fractional Fourier transform to compute the cross correlation (GCC -FRFT) . Image quality factors of the elastograms obtained using the different TDE techniques are analyzed and the results are compared using standard statistical tools.

The results of this research suggests that correlation based techniques outperform SSD and SAD techniques in terms of SNR_e, CNR_e, dynamic range and robustness. The sensitivity of GCC-FFT and SSD were statistically similar and statistically higher than those of all other methods. Within the class of GCC methods, there is no statistically significant difference between SNR_e of GCC-FFT, GCC-PE and GCC –FRFT for most of the strain values considered in this study. However, in terms of CNR_e, GCC-FFT and GCC-FRFT were significantly better than other TDE algorithms. Based on these results, it is concluded that correlation-based algorithms are the most effective in obtaining high quality elastograms.

To my parents

ACKNOWLEDGEMENTS

I would like to thank my Committee Chair, Dr. Raffaella Righetti for being extremely kind and supportive throughout the course of this research. My thanks to my colleagues at the lab, Raghavendra Desai, Sthiti Deka and Xu Yang, for their technical inputs and suggestions. I am grateful to my committee members, Dr. Jim Ji, Dr. Deepa Kundur and Dr. Javier Jo, for their guidance and support.

My thanks to Ms. Prabha Acharya for giving me the opportunity to work as a Graduate Assistant in the Texas A&M University Library. Thanks also go the department faculty and staff for making my time at Texas A&M University a great experience.

Finally, this work would have been impossible but for the love and support showed by my family and friends. My sincere thanks to all of them.

TABLE OF CONTENTS

CHAPTER Page

LIST OF FIGURES

FIGURE Page

LIST OF TABLES

CHAPTER I

INTRODUCTION

Ultrasound Elastography is a non-invasive medical imaging modality that provides the distribution of local strains experienced by soft tissues due to compression [1], [2]. The resulting strain images are referred to as “elastograms”. Elastography is currently used as a diagnostic tool in detecting pathological changes in soft tissues [1].

A. Motivation

Pathological changes are usually associated with changes in tissue’s mechanical properties [2]. Palpation is one of the preliminary methods in detecting tumors. Palpation is subjective and does not allow the classification of tumors [2]. Alternatively, a physician can use medical imaging techniques or biopsy, which is a costly and painful invasive procedure.

Ultrasonic B-mode imaging is an established medical imaging tool that is used in a variety of clinical applications [2]. Malignant or Benign tumors may have echogenic properties which might make them undetectable in conventional B-mode ultrasonic images [2]. However, cancerous tissues may be several times harder than the surrounding soft tissues [3]. Therefore imaging tissue stiffness or related parameters can

---

The journal model is *IEEE Special Issue on Systems Biology*.

serve as a tool to diagnose cancers and possibly distinguish between benign and malignant tumors [2]. For example in the case of a breast tumor, a benign tumor may be several times softer than a malignant one [3]. Since the echogenicity and the stiffness of tissue are unrelated properties, imaging tissue stiffness or strain will provide new additional information that is related to pathological tissue structure [2].

Elastography methods aim at imaging the local strains that a tissue experience under quasi-static compression [1] [2]. Local strains are usually estimated as the gradient of local tissue displacement, which are computed from the time delays between gated pre- and post-compression echo signals. The quality of the resulting elastograms is highly dependent on the accuracy and precision of these local displacement estimates [4]. While several time delay estimation (TDE) techniques have been proposed for elastography applications, there is a lack of systematic study that statistically compares the performance of these techniques. This information could prove of great importance to improve currently employed elastographic clinical methods.

Therefore, the primary motivation of this work is to provide a solid understanding of potentials and limitations of several TDE techniques for elastography applications so that quality elastograms can be produced and used in conjunction with ultrasound B- mode images as a reliable diagnostic tool.

B. Research Plan

Elastography is traditionally implemented by first estimating the displacement between a pair of reflected RF echo signals [2]. Often, cross correlation methods are used to

estimate these displacements. Thereafter, the local strains are computed from the estimated displacement using gradient methods [2]. In addition to correlation, there are many other methods that can be used for time delay estimation (TDE). This thesis explores a number of TDE elastography methods. Specifically the aim of this work is as follows:

1. Develop software that generates the axial and lateral displacement maps and axial and lateral elastograms.

2. Implement different Time Delay Estimation (TDE) algorithms. These are based on generalized cross correlation, Sum of Squared Differences (SSD) [5], Sum of Absolute Differences (SAD) [5]. Within the class of GCC algorithms, an FFT-based cross correlation algorithm (GCC-FFT), a hybrid time-domain and frequency domain cross correlation algorithm with prior estimates (GCC-PE) and a new algorithm based on the use of fractional Fourier transform (GCC-FRFT) are implemented. It should be noted that the use of fractional Fourier transform for elastography applications has never been reported so far.

3. Perform statistical analysis on the performance of the algorithms, in terms of elastographic signal-to-noise ratio (SNR_e), elastographic contrast-to-noise ratio (CNR_e), sensitivity and dynamic range and computational time. The performance is evaluated for a range of applied strain values. The results are statistically compared using standard statistical tests.

C. Structure of the Thesis

Chapter II discusses the basic and concepts and the various steps involved in obtaining an elastogram

Chapter III provides the methods and implementation of the various TDE algorithms that are considered in this study.

Chapter IV discusses the performance indicators used for quantifying image quality of elastograms. It also provides the results of the image quality analysis and the statistical analysis.

Chapter V presents the conclusions and the avenues for future work in this area.

CHAPTER II

ELASTOGRAPHY

Elastograms represent maps of local tissue strains experienced by a tissue under quasi-static compression. Local tissue strains are related to the underlying mechanical properties of the tissue, which depend on the molecular building blocks of the tissue and on the structural organization of these blocks [2]. In order to image the mechanical behavior of a tissue, a mechanical stimulus of some kind must be propagated into the tissue and precision means for detecting internal tissue motion must be provided. Imaging tissue's mechanical properties is a challenging task due to the difficulty in describing a tissue's behavior using mathematical models. For creating a simple, viable mathematical model of the behavior of a tissue, certain assumptions have to be made [2].When the mechanical stimulus is propagated through the tissue for a very short duration (ideally an impulse), it can be assumed that the response of the tissue only depends on the current applied stimulus and not on any previous loading. The viscosity of the tissue can then be ignored and the tissue can then be assumed to be an elastic material [2].

Now that the tissue has been approximated to a perfect elastic material, when a quasi static uniaxial compression is applied [5], [4], [6], [2], all the particles in the medium will experience a longitudinal strain along the direction of the applied compression. Harder tissue regions experience lower strains whereas softer tissue

regions experience higher strains. In elastography, the local tissue strain maybe defined as [2]:

$$\epsilon = \frac{d_1 - d_2}{\Delta t} \tag{2.1}$$

where ϵ denotes the strain , d_1 and d_2 denote the time delay estimates of observation windows 1 and 2 respectively at any time t and $t + \Delta t$.

A. Steps to Obtain an Elastogram

In order to obtain a map of the distributions of these strains (i.e., an elastogram) several steps must be executed. Fig 1 shows the steps required for obtaining an elastogram.

1. Pre and Post Compression Data Acquisition

Prior to tissue compression, a set of digitized Radio Frequency (RF) echo lines are obtained from the tissue of interest using a standard diagnostic ultrasound system (pre-compression frame).Then the tissue is slightly compressed using the ultrasonic transducer, and another set of RF echo lines are obtained from the same tissue area of interest (post-compression frame). It is important to note that the compression is usually a very small percentage of the tissue depth (<1%), typically less than one mm.

2. Global Temporal Stretching

Due to the compression of the tissue, echoes obtained from acoustic scatterers in the tissue are distorted. Thus, the post compression echo signals are not just the exact

delayed version of the pre compression echo signals. This distortion (which constitutes the actual strain) is a major cause of loss of correlation between the pre and post compression signal. This effect is known as echo signal decorrelation, and it is one of the

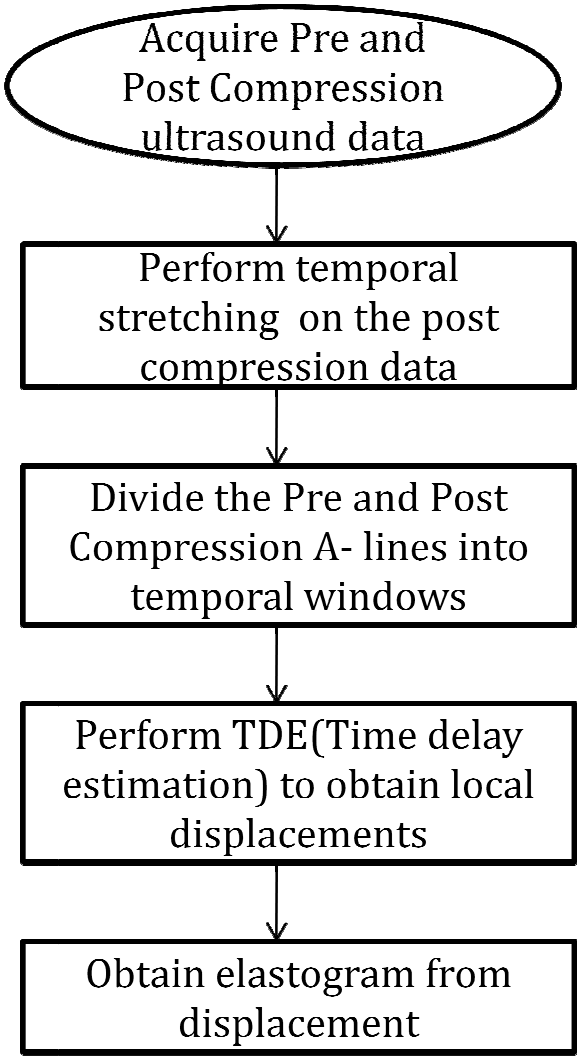

Fig. 1. Schematics of the steps necessary to obtain an elastogram.

important factors that limit the quality of elastograms [7]. Therefore, the echo-signal decorrelation should be minimized to obtain a meaningful estimation of tissue displacement.

In order to limit this decorrelation, a global stretching [7] is usually performed on the post compression frame prior to time delay estimation. In global temporal stretching, all post compression echo lines are stretched equally by the same strain magnitude as the strain applied during compression. This method is computationally inexpensive and also significantly improves the correlation between pre and post compression signals hence leading to improved displacement map estimation. Temporal stretching basically realigns the pre and post compression signals, and it is implemented using linear interpolation.

3. Time Delay Estimation

The estimation of the time delay between the pre and post compression temporally stretched signals is perhaps the most important step in the generation of an elastogram, and the one that mostly affects the quality of elastograms [4]. Time delay occurs due to spatial shift in the tissue caused by its compression. If the velocity of sound in the tissue is assumed to be constant, the time delay is directly proportional to the spatial shift in the tissue. Thus by estimating the time delay, the spatial shift can also be estimated.

Time delay estimation can be performed in many different ways and several methods are considered in this study. In all the methods considered in this study, congruent echo lines from the pre and post compression signals are divided into several

temporal windows of equal length and their time delay is estimated using the different algorithms. The window length is an important parameter in determining the quality of the elastogram and it has to be a function of the ultrasonic wavelength [8]. The windows are translated in small overlapping steps along the axial direction [2]. This is repeated for all the depths and for all the A-lines to obtain the complete displacement map. The different time delay estimation algorithms are discussed in detail in Chapter III.

The estimates obtained using the TDE algorithms are coarse and to obtain a finer sub sample displacement, either oversampling or interpolation techniques can be used [2]. In this work, a parabolic interpolation is used to obtain sub sample displacement [9]. Parabolic interpolation is a quadratic interpolation method that fits a parabola to the function at three unique points (maximum value and the one prior and after the maximum value). The new displacement is obtained as the peak value of the fitted parabola.

Prior to strain estimation, the obtained displacement map is then usually median filtered to remove salt-and-pepper noise in the displacement map.

4. Strain Estimation

Strain distribution image or elastogram is obtained from the displacement map. One simple method of obtaining an elastogram is to compute the gradient of the displacement map [2]. However, this method provides very noisy strain estimates which result in low elastographic SNR as can be seen in Fig 2(b). Other more advanced techniques have

been proposed to estimate strain. Among these are: the staggered strain estimation [10] and the least squares strain estimator [11].

Staggered strain estimator uses a multi step strain estimation technique [10]. It first computes the strain by computing the gradient of displacements between non overlapping adjacent windows rather than successive overlapping windows as in the case of the simple gradient method. Subsequently, windows are shifted by a fraction of the window length and strain is estimated for non-overlapping windows with this window translation. This is repeated till the cumulative window shift equals or exceeds the window length. The results from all the iterations are staggered [10]. The obtained gradient is the strain estimate of that particular window. This process is repeated for one particular A-line and then for all the A-lines to obtain the elastogram. This method significantly improves the quality of image and eliminates a number of noisy strain estimates [10]. Fig 2(c) shows an elastogram obtained using staggered strain estimation method.

Least squares strain estimator estimates the strain by making a piece wise linear fit of the displacement data of the displacement map to obtain the strain [11]. This method is also shown to considerably improve the elastographic SNR, but at the expenses of spatial resolution [11]. This method is the one of choice for the statistical study reported in this thesis, due to its simplicity and the fact that is widely applied in elastography studies. Therefore, below, we summarize the major steps necessary to estimate the strains using a least squares strain estimator.

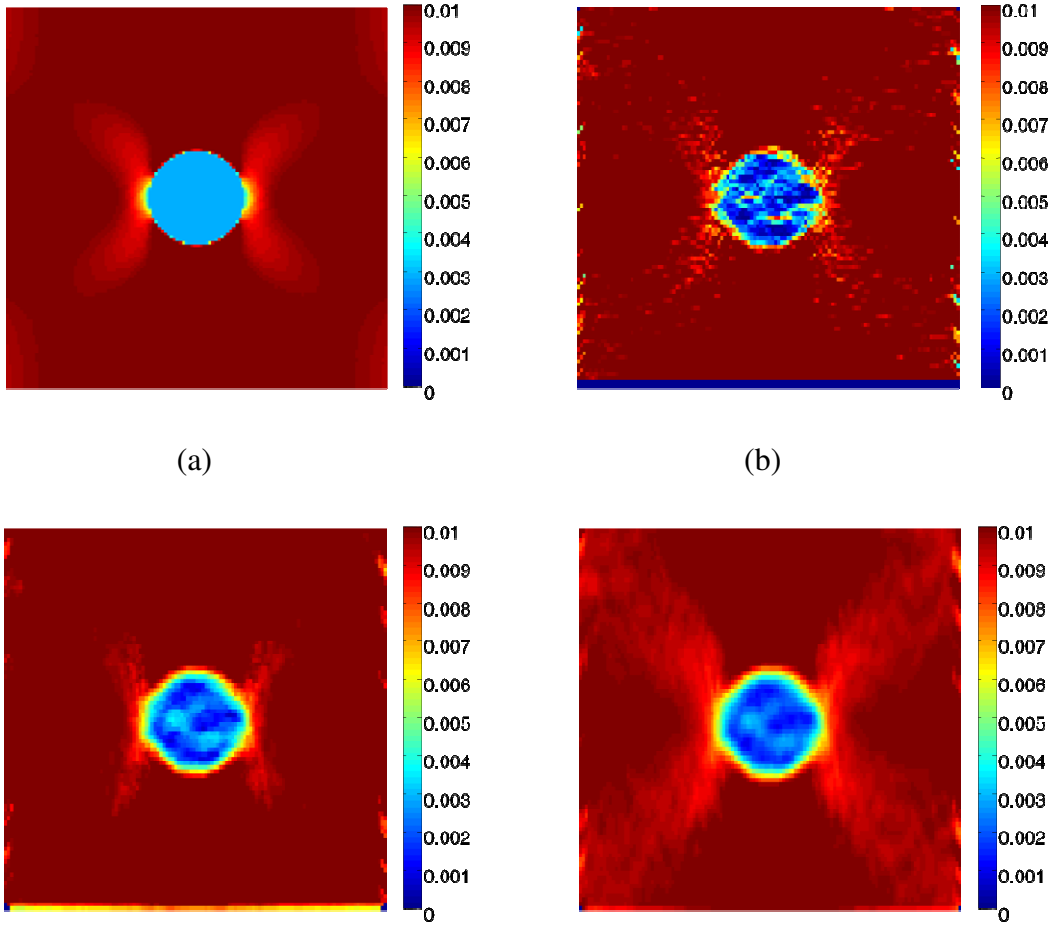

Fig. 2. Elastograms of a simulated medium containing a hard inclusion at 1% applied strain. (a) Ideal simulated strain distribution map. (b) Elastogram obtained using a simple gradient strain estimation method. (c) Elastogram obtained using a staggered strain estimation method. (d) Elastogram obtained using a least squared estimation method.

The displacement estimates around a small kernel N can be modeled as

$$d(i) = a.z(i) + b \text{ for } i = 1 \ldots N \tag{2.2}$$

where

d : displacement estimates

z : tissue depth

N : size of the kernel

a,b : constants to be estimated.

Equation 2.2 can be written in matrix form as

$$d = A.\begin{bmatrix} a \\ b \end{bmatrix} \tag{2.3}$$

where A is a N x 2 matrix where the first column represents the depth position z (i) and the second is a column of ones.

$$\begin{bmatrix} a \\ b \end{bmatrix} = A^T [\, A.A^T \,]^{-1} \cdot d \tag{2.4}$$

The quantity ‘a’ represents the strain estimate.

B. Summary

In this chapter, we described the necessary steps that must be performed in order to obtain an elastogram. The different Time delay estimation techniques are critical in obtaining a high quality elastogram, and they form the central portion of this thesis. A selection of different TDE techniques is discussed in the next chapter. The method used to estimate the strains from the local displacements is also important. In this chapter, we summarized several methods, with particular emphasis on the least squares strain estimator, which has been used in this thesis for performing the statistical study.

CHAPTER III

TIME DELAY ESTIMATION ALGORITHMS

A. Problem Formulation

Time delay estimation (TDE) is a classical problem which appears in a variety of applications like audio signal processing, wireless communications and biomedical signal processing etc [5]. As discussed in the previous chapter, time delay estimation is also a critical step in the generation of an elastogram. It can be formulated as follows:

Let $r_1(t)$and $r_2(t)$ be random processes that represent the reference and the delayed signals, $s(t)$ be the pulse echo point spread function of the imaging system, $h_1(t)$ is the tissue scattering function and $h_2(t) = h_1(at)$ where a $= \frac{1}{1-\epsilon}$,where ϵ is the applied strain. $n_1(t)$ and $n_2(t)$ represent additive noise processes introduced from electronic sources [7]. Then, $r_1(t)$ and $r_2(t)$ can be written as:

$$r_1(t) = h_1(t) * s(t) + n_1(t) \tag{3.1}$$

$$r_2(t) = h_2(t) * s(t) + n_2(t) \tag{3.2}$$

Fig 3 shows the time delay between the pre and post compression A-lines obtained in ultrasound elastography. There are several methods for estimating the delay between $r_1(t)$ and $r_2(t)$ .The central work of this thesis consists of implementing the various time delay estimation algorithms and investigating their performance in terms of elastogram image qualities. In the next sections, a detailed technical description of each of the TDE method implemented in this study is provided.

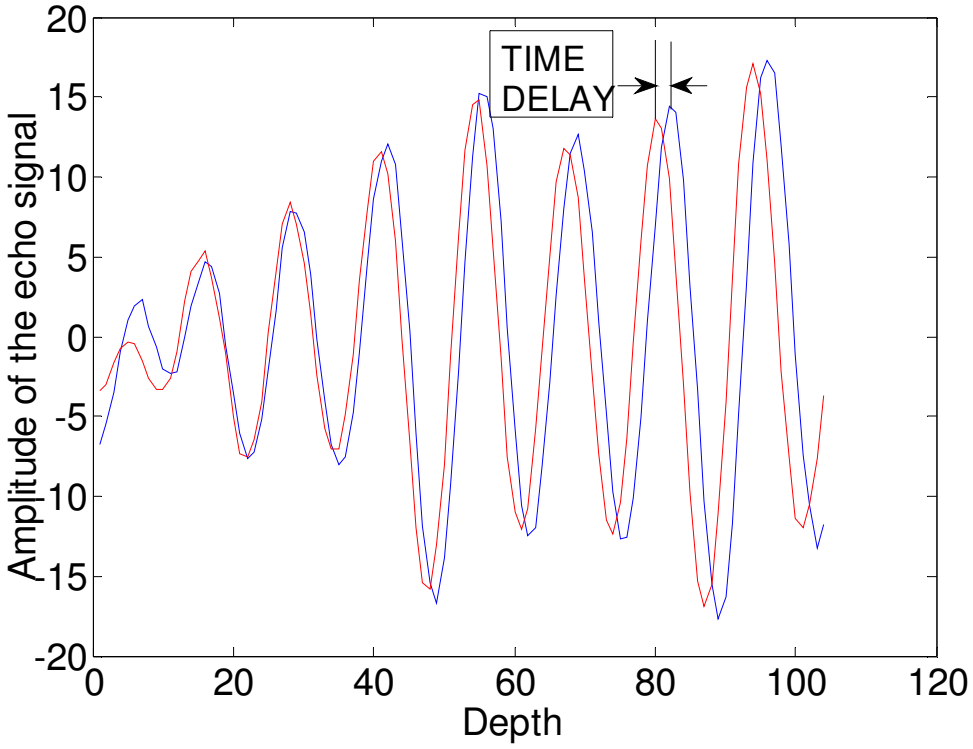

Fig. 3. Example of pre and post compression windows.

B. Generalized Cross Correlation-Fast Fourier Transform (GCC-FFT)

Generalized Cross Correlation is one of the most effective methods used in time delay estimation because it is computationally less complex and provides accurate time delay estimates [2]. In this method, the cross correlation function between the pre and post compression windows is computed. The estimated delay is obtained by finding the time-lag that maximizes the cross-correlation between the two signals. The expression for cross correlation is given by [12]:

$$R(\tau) = E[\, r_1\ [n]\, r_2\, [n+\tau]\,] \tag{3.3}$$

$$= \frac{1}{N} \sum_{i=1}^{N} r_2 [\, i \,]\, r_1 [\, i + \tau]$$ (3.4)

where

r_1 : Pre compressed signal window

r_2 : Post compressed signal window

$R\ (\tau\ )$: Cross Correlation function between pre and post compressed signal windows.

τ : Time delay between pre and post compressed signal window.

N : Number of samples in a window

A schematic of the GCC-FFT method is shown in Fig. 4.

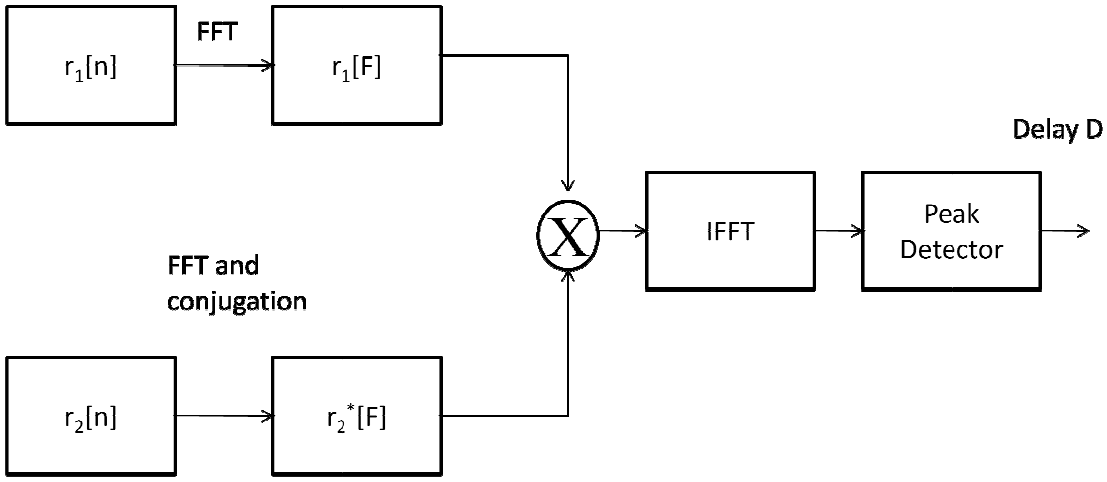

Fig. 4. Schematic of the GCC-FFT method.

A definitive indicator of the accuracy of the time delay estimate is the normalized cross correlation coefficient which is obtained by normalizing the cross correlation function by the product of peaks of autocorrelation function of the pre and post compressed window [4]. The time shift error in the normalized cross-correlation function is significantly lower than in the unnormalized cross-correlation function and hence is preferred over the unnormalized cross-correlation function [13]. Usually, the cross correlation is carried out in frequency domain and not in time domain because it is more computationally efficient.

In the frequency domain, the cross correlation function is found out as the inverse Fourier transform of the product the FFT of the pre compression window and the conjugation of FFT of the post compression window. FFT implementation takes only logarithmic time complexity (while it would take quadratic time complexity o (n^2) to perform cross correlation in time domain). The position of the peak of the cross-correlation function yields the time-delay estimate. This process is repeated for all the windows and for all the A-lines to obtain a complete displacement map. An example of simulated displacement map obtained using the GCC-FFT is shown in Fig. 5.

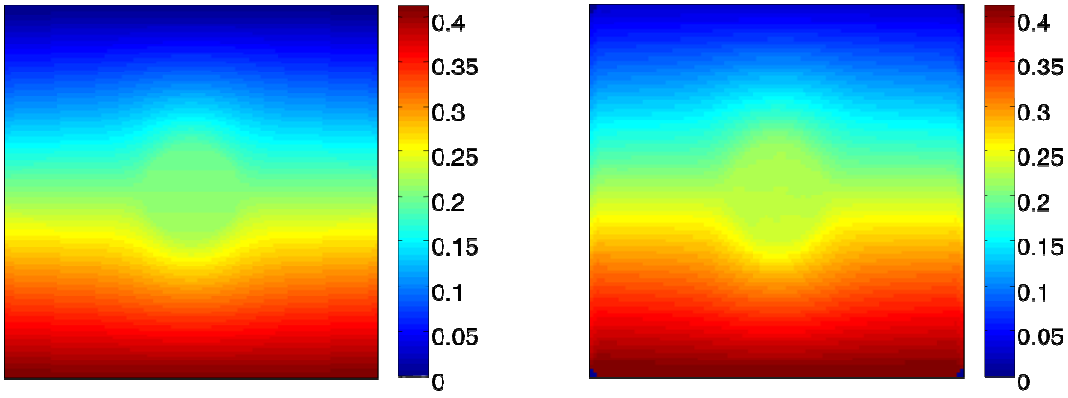

(a) (b)

Fig. 5. (a) Example of ideal displacement map obtained from a simulated medium containing a hard inclusion at 1 % applied strain. (b) Corresponding estimated displacement map obtained using GCC-FFT algorithm (after median filtering).

C. Generalized Cross Correlation with Prior Estimates (GCC-PE)

Generalized Cross Correlation with prior estimates algorithm makes use of the fact that neighboring regions of the tissue are almost the same biologically and undergo similar displacements when subjected to compressive strain [14]. This fact can be exploited to reduce the amount of computations necessary to obtain the displacement map. Typically, this algorithm makes use of only 3 values of lags within a predicted region to make an estimate of the displacement of a window [14]. In order to obtain the displacement map, the displacements of the windows are calculated in a manner very similar to that of raster scan [14]. The displacement of the very first window in the first row is calculated using the generalized cross correlation method. Now the position of the peak of the correlation function is stored. The value of the position of the peak is used to obtain the correlation

value for next window (to the right of the current window) only at that particular value. The correlation values are computed for positions preceding and succeeding the predicted peak. These values are used for parabolic interpolation and the improved correlation coefficient is obtained. This is repeated to obtain the time delay estimates of the entire first row and similarly repeated for all other rows to obtain the complete displacement map.

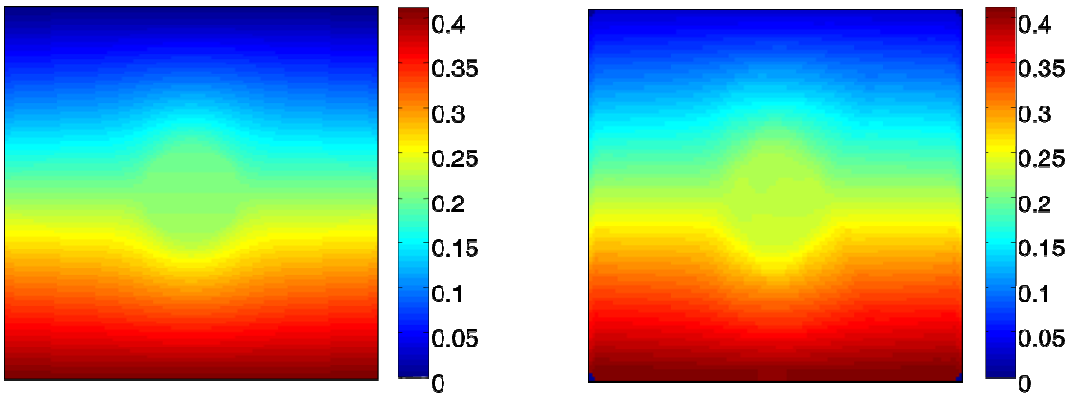

(a) (b)

Fig. 6. (a) Example of ideal displacement map obtained from a simulated medium containing a hard inclusion at 1 % applied strain. (b) Corresponding estimated displacement map obtained using GCC-PE algorithm (after median filtering).

The prediction of the search bracket from one window to the next may generate occasional errors. These errors could be due to a multitude of reasons like a region that is

a boundary between hard and soft part of a tissue. In those cases, predicted position may turn out to be incorrect. An array with the values of the predicted position of the peak is maintained. If the prediction turns out to be correct (a threshold of 0.9 is used in the implementation), the value of the prediction array is updated with the previously predicted position value. In case the prediction is poor, the value of correlation coefficient is lower than the threshold, the predicted value is discarded and the displacement is computed using the standard generalized cross correlation TDE method and that position of the peak is used for the next prediction and so on. This search is carried out only if the prediction fails .This ensures that the standard algorithm is run only for a small region and not on the entire RF data as it was done earlier. On analysis with different test samples, the recovery search (search to find out the peak when prediction failed) to find the new peak was triggered on an average only in 2-3 % of all the windows. This drastically reduces the time required to obtain the displacement map. However, in highly heterogeneous tissues, this number could be significantly higher. An example of simulated displacement map obtained using the GCC-PE is shown in Fig. 6.

D. Fractional Fourier Transform

Fractional Fourier Transform is a linear transformation which is a generalization of the Fourier Transform. Fractional Fourier transform [15] of a signal f (t) is defined as

$$F_a(\omega) = \sqrt{(1 - j.\cot\alpha)\frac{1}{2\pi}}.e^{j\cot(\alpha).\frac{\omega^2}{2}}. \int_{-\infty}^{\infty}[e^{-j\csc(\alpha)\omega t+\frac{jcot(\alpha)t^2}{2}}].f(t)dt \quad (3.5)$$

where α = a. π/2 and ω is the complex frequency;

The kernel inside the square rackets in Eq 3.5 is a chirp function and hence the above transformation can be interpreted as a coordinate transformation in which the chirp functions play the role of basis functions.

a) When a =1, i.e. $\alpha = \pi/2$, the Fractional Fourier transform simplifies as

$$F_a(\omega) = \frac{1}{\sqrt{2\pi}} \int_{-\infty}^{\infty} \mathrm{f(t)} \exp\left(-\mathrm{j}\,\omega t\right) dt$$

which is the conventional Fourier transform.

b) When a = 0, the equation simplifies to the identity operation, which is the time domain signal itself.

Fractional Fourier Transform provides an additional parameter ‘a’ when compared to the traditional Fourier transform. This parameter ‘a’ provides more flexibility as compared to the traditional Fourier transform, which can be utilized in many applications. For any value of ‘a’ between 0 and 1, Fractional Fourier transform can be imagined as the rotation of the signal which is determined by the parameter ‘a’ in the time-frequency axis, thus giving a transform domain which gives both time and frequency information [15]. Thus, Fractional Fourier transform based estimators are linear estimators which are of much broader class than the Fourier transform based Generalized cross correlation estimators.

One of the significant applications of Fractional Fourier transform is in the area of signal filtering and estimation [16]. The reasoning behind using Fractional Fourier transform for filtering is that there are circumstances where elimination of noise is not possible just either in time domain or frequency domain while it is possible in certain Fractional Fourier transform domain [16].

While the use of FFT to obtain time delay estimates is optimal when the system and signals involved are time invariant, it may not be optimal for time varying signals and systems [16]. Thus in this study, we explore the use of FRFT for elastography applications, which has never been proposed so far. A schematic for obtaining the peak of fractional correlation is shown in Fig 7.

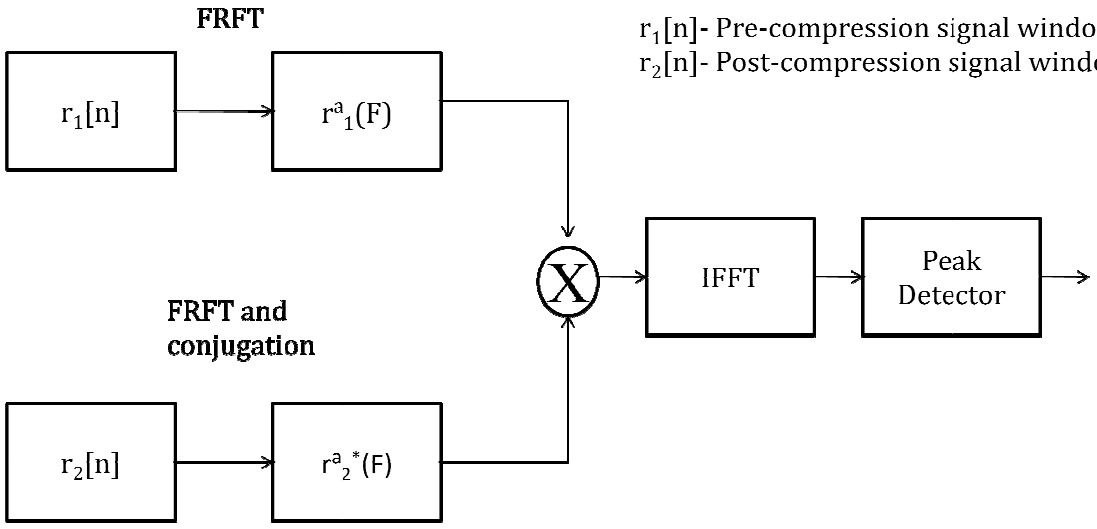

Fig. 7. Schematic for obtaining the peak of fractional correlation.

To find the optimal value of 'a', we compute fractional correlations [17] for values of 'a' evenly spaced out between 0 and 1 is found out. Fractional correlation is computed by taking the Fractional Fourier transform of pre compression window and multiplying it with the conjugated Fractional Fourier transform of post compression

window, and by finally performing a conventional inverse Fourier transform on the obtained product [17]. The value corresponding to the peak of all fractional correlation coefficient is stored in an array and the maximum of all the peaks of all fractional correlation coefficient is used as the correct estimate of displacement. An example of simulated displacement map obtained using the GCC-FRFT is shown in Fig. 8.

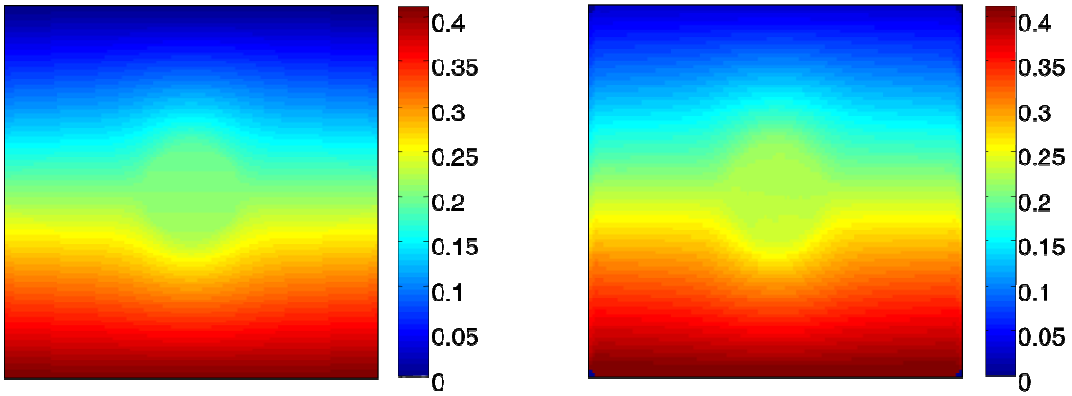

(a) (b)

Fig. 8. (a) Example of ideal displacement map obtained from a simulated medium containing a hard inclusion at 1 % applied strain. (b) Corresponding estimated displacement map obtained using GCC-FRFT algorithm (after median filtering).

E. Sum of Squared Differences (SSD) and Sum of Absolute Differences (SAD)

Sum of Squared Differences (SSD) and Sum of Absolute Differences (SAD) are TDE algorithms where the displacement is found out by measuring the delay that minimizes L_2 (Euclidean distance) and L_1 (Taxicab or Manhattan norm) norms respectively

between the pre compression and the post compression signals [5]. The implementation of this method is similar to that of the generalized cross correlation method except that the part of the code where correlation is computed is essentially replaced with the computation of SSD or SAD. The SSD and SAD functions can be expressed as [7]:

$$R_{SSD}(\tau) = \sum_{n} [r_1(n) - r_2(n+\tau)]^2 \tag{3.6}$$

$$R_{SAD}(\tau) = \sum_{n} [r_1(n) - r_2(n+\tau)] \tag{3.7}$$

The time delay is computed by finding the value of the delay τ that minimizes the SSD or the SAD functions, viz:

$D = \arg_{\tau} min\ [R_{SAD}\ or\ R_{SSD}\ ]$. An example of simulated displacement map obtained using the SSD is shown in Fig. 9.

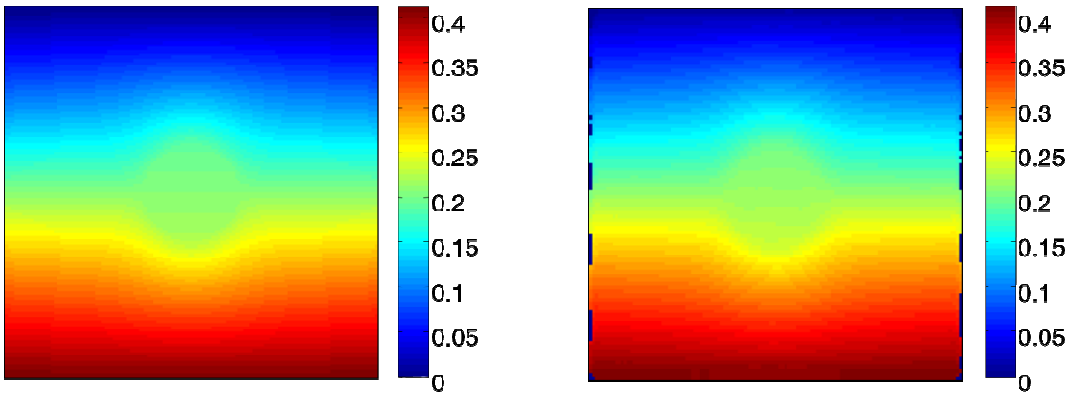

(a) (b)

Fig. 9. (a) Example of ideal displacement map obtained from a simulated medium containing a hard inclusion at 1 % applied strain. (b) Corresponding estimated displacement map obtained using the SSD algorithm (after median filtering).

An example of simulated displacement map obtained using the SAD is shown in Fig. 10.

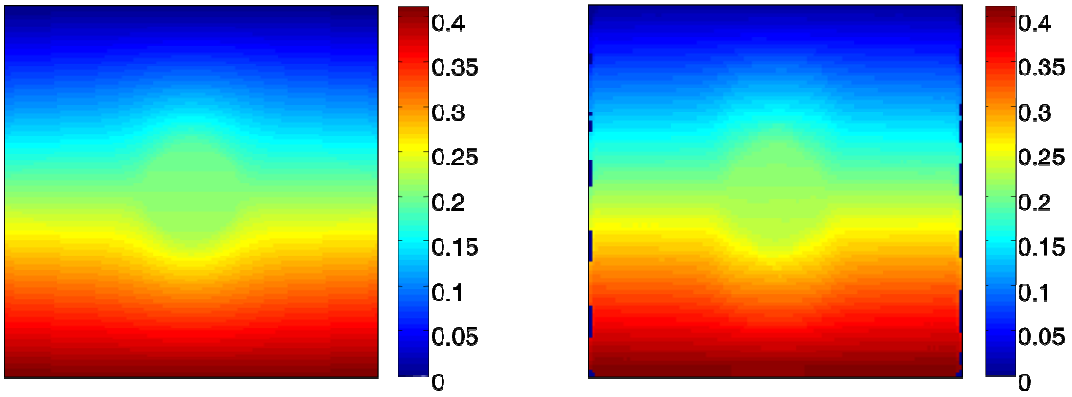

(a) (b)

Fig. 10. (a) Example of ideal displacement map obtained from a simulated medium containing a hard inclusion at 1 % applied strain (b) Corresponding estimated displacement map obtained using the SAD algorithm (after median filtering).

F. Summary

In this chapter, a selection of different TDE algorithms was discussed. The TDE methods implemented in this thesis are widely used in clinical elastography applications and they are all based on a cost function. We have provided the detailed techniques used to implement these methods. The implemented TDE methods can provide both axial and lateral displacement maps. From the displacement maps obtained using these TDE

algorithms, elastograms can be obtained using the strain estimation methods explained in the previous chapter. In the next chapter, we perform a comprehensive image quality analysis of the axial strain elastograms obtained using the various TDE methods described in this chapter. Results obtained using different image quality indicators will be analyzed using standard statistical methods.

CHAPTER IV

PERFORMANCE INDICATORS AND RESULTS

In order to compare the performance of the different time day estimation techniques implemented in this thesis, a study was carried out by applying the time delay estimation algorithms to media with different mechanical properties which were simulated. Using the obtained elastograms, an image quality analysis was performed. The quality of the elastograms was quantified using image quality factors typically used in elastography studies [2]. These include: the elastographic signal-to-noise ratio (SNR_e), the elastographic contrast-to-noise ratio (CNR_e), sensitivity and dynamic range. In this study, the spatial resolution was not evaluated as the elastographic spatial resolution is fundamentally limited by the physics of the ultrasound system and the window length (which was kept the fixed in the implementation of the TDE techniques) [8].

In general, the image quality factors in elastography obtained depend on the following parameters:

1. Quality of Time Delay Estimates obtained from various TDE algorithms [13].
2. Transducer Parameters. (Transducer center frequency, Bandwidth, Beamwidth, Sampling frequency) [2].
3. Signal Processing Parameters. (Length of the window, Percentage of overlap) [2], [18].
4. Mechanical Parameters. (Elastic modulus, Poisson's ratio) [2].

The transducer, signal processing and mechanical parameters are interdependent and their values must be chosen together in such a way so as to obtain a quality elastogram [2]. For example, the window length (signal processing parameter) must be a function of ultrasound wavelength (transducer parameter). A change in transducer parameters should influence the signal processing parameters as well. In this study, the transducer, signal processing and mechanical parameters are fixed for all algorithms to evaluate image quality of the various TDE algorithms under the exact same conditions.

A. Image Quality Parameters

The parameters that are used to determine the quality of the obtained elastographic image are

1. Elastographic Signal-to-noise Ratio (SNR_e) [8].
2. Elastographic Contrast-to-noise Ratio (CNR_e) [8].
3. Elastographic Dynamic Range [4].
4. Elastographic Sensitivity [2].
5. Computational Time.

1. Elastographic Signal-to-Noise Ratio

Signal to noise ratio is a measure of the signal strength (or power) relative to the noise. The elastographic SNR has been defined as [8]

$$SNR_e = \frac{\mu}{\sigma} \tag{4.1}$$

where μ is the mean of the strain in the area of interest in the elastogram and and σ is the standard deviation of the strain in the area of interest in the elastogram. SNR_e is usually computed from uniform media (or uniform regions of strain in the material).

Related to the notion of SNR_e is an elastographic theoretical framework, which has been referred to in the literature as "Strain Filter" [19]. The strain filter is the plot of the upper bound of achievable SNR_e as a function of the applied strain. The strain filter has a typical bandpass characteristic in the strain domain, indicating that there exist a range of applied strains for which the SNR_e is maximized. At low values of applied strains, the SNR_e is limited by electronic noise effects and at high values, it is limited by signal decorrelation [19]. Each strain filter curve depends on the signal processing and system parameters used to obtain the elastogram [19].

The strain filter concept can also be extended to predict elastographic CNR and dynamic range at a given resolution in terms of the signal processing and system parameters used to obtain the elastograms [19]. Thus, the strain filter can be used to quantify the performance of a Time delay estimation algorithm by providing graphically various image quality parameters.

2. Elastographic Contrast-to-Noise Ratio

Contrast to noise ratio quantifies the ability to distinguish between differences in intensity in an image.

The elastographic CNR is defined as [8]

$$CNR_e = \frac{2(\mu_t - \mu_b)^2}{\sigma_t^2 + \sigma_b^2} \quad (4.2)$$

where μ_t and μ_b are the mean values of the estimated strain in the target and the background respectively, and σ_t and σ_b are the respective standard deviation of the estimated strains.

3. Elastographic Dynamic Range

Dynamic range [13] in elastography is defined as the difference between the maximum measurable strain and the minimum measurable strain at a given SNR_e. In dB, this ratio can be expressed as:

$$DR_e = 20 \log \frac{strain_{max}}{strain_{min}} \quad (4.3)$$

Where $strain_{min}$ and $strain_{max}$ are the minimum and maximum measurable strain, respectively, at a given SNR_e. For this study, the dynamic range was computed at an SNR_e = 30 dB and using Eq 4.3.

4. Elastographic Sensitivity

Sensitivity is defined as the minimum measurable applied strain at a given value of SNR_e [13]. Sensitivity value quantifies the performance of the time delay estimation algorithm at low values of applied strain. For this study, the dynamic range was computed at an SNR_e = 30 dB.

5. Computational Time

Computational time was estimated on a pixel basis to evaluate the time required for each of the algorithm to compute a pixel in the elastogram on a computer that runs on a Intel ® Core ™ 2 Duo CPU @ 2 GHz and 2 GB RAM. The algorithms were implemented using MATLAB (Mathworks, Inc., Natick, MA, USA).

B. Simulation Study

In order to evaluate the performance of the various time delay algorithms, a simulation study was carried out. The Finite-element (FE) simulated media were generated using a commercial software package (Comsol Multiphysics 3.5a, Comsol Inc., Palo Alto, CA). Each phantom had dimensions of 40 mm x 40 mm x 40 mm and was compressed from the top. Slip boundary conditions at the bottom and a plane-strain state model was assumed. Several models of simulated media were generated: uniform phantoms (for the SNR_e study) and phantoms containing an inclusion (for the CNR_e study). Fig 11 shows the ideal strain distribution of a uniform medium (a) and a medium containing a hard inclusion (b).

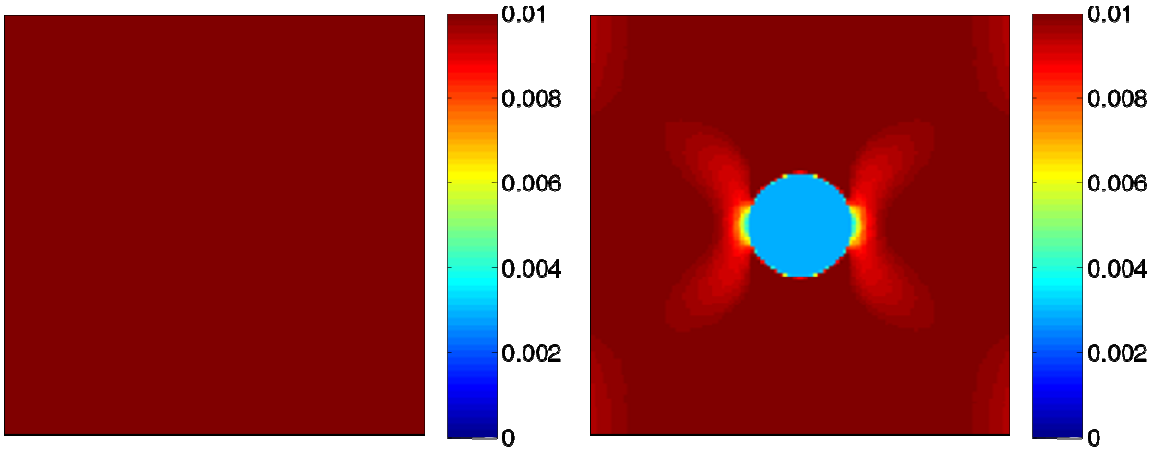

(a) (b)

Fig. 11. Ideal strain images of (a) The uniform simulated medium used for the SNR_e study (b) The medium containing a hard inclusion used for the CNR_e study.

The SNR_e was measured on simulated uniform cubic phantoms (elastic modulus = 2 kPa and Poisson's ratio = 0.49). The CNR_e was measured on simulated cubic phantoms containing a 10 mm diameter cylindrical inclusion (background: elastic modulus = 2 kPa and Poisson's ratio = 0.49; inclusion: elastic modulus = 10 kPa and Poisson's ratio = 0.49). The mechanical simulation software provided us with the values of displacements at each node in the phantom. The displacements obtained from the mechanical models were then used to create the pre- and post-compression simulated RF data using dedicated ultrasound simulation software routines created in our laboratory.

In all models, a scatterer density of at least 40 scatterers / pulse-width was used, satisfying the requirement for obtaining fully developed Rayleigh backscatterers. The

speed of sound was fixed at 1540 m/s (speed of sound in tissues). The sonographic signal-to-noise ratio (SNR_s) was set at 20 dB by adding other uncorrelated RF A-lines to both the pre- and post-compression A-lines. The parameters of the simulated ultrasound transducer had 128 elements, a 6.6 MHz center frequency and 50% fractional bandwidth at -6 dB, 1 mm beamwidth and 40 MHz sampling frequency.

The performance of the various TDE algorithms implemented in this study is compared at applied strains ranging from 0.01 % to 10 %. To study the effects of the window length on the resulting elastograms, different window lengths were considered (0.5 to 4 mm). The window overlap was fixed at 80% the window length. The stretching factor was assumed to be equal to the applied strain. From the simulated pre and post compression RF signals, displacement maps were obtained using the various TDE algorithms. In all cases, least squares strain estimation method was used to obtain the elastogram. For statistical purposes, 50 independent realizations were used for each case considered.

C. Experimental Validation

In addition to simulations and as a proof-of-principle, the applicability of the various TDE techniques implemented in this study was tested on a set of experimental RF data obtained from a tissue mimicking phantom. These experimental data were acquired using a 38 mm real-time linear array scanner Sonix RP (Ultrasonix, Richmond, BC, Canada) that has 128 elements, a bandwidth between 5-14 MHz, a center frequency of

6.6 MHz, 50% fractional bandwidth at -6 dB, sampling frequency of 40 MHz, applied strain percentage of 0.001 % and 1 mm beamwidth at the focus.

D. Statistical Analysis of Results

Statistical comparison of the results (SNR_e, CNR_e, Sensitivity and Dynamic Range) obtained from the different TDE techniques were performed using t-testing and confidence interval bounds [12].

E. Simulation Results

Fig 12 shows examples of elastograms obtained using the various TDE methods implemented in this study as applied to the uniform simulated medium at a 5% applied strain.

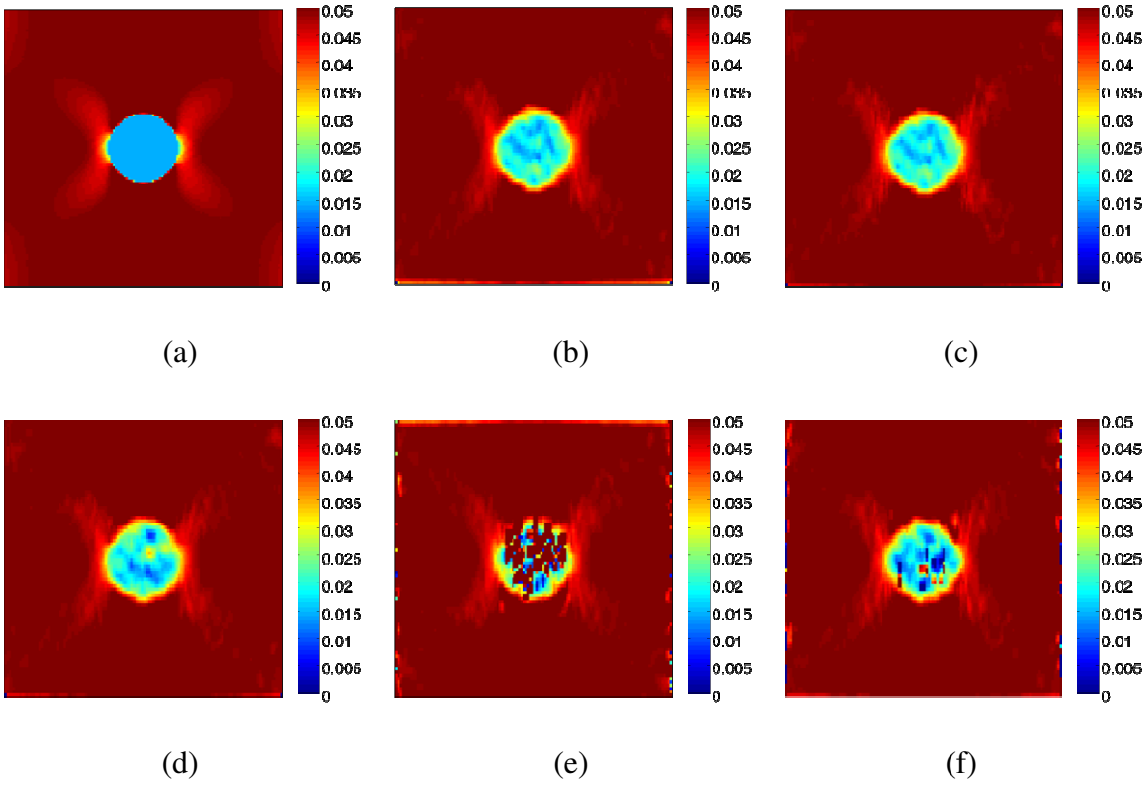

Fig. 12. (a) Ideal strain image at 5% applied strain. Elastograms obtained using (b) GCC-FFT (c) GCC-PE (d) GCC-FRFT (e) SSD (f) SAD.

Figs. 13-18 show the effect of window length (0.5 mm, 2 mm, 4 mm) on the estimated strains using the various TDE algorithms implemented in this study (at a 1% applied strain). The improvement of CNR_e as well as corresponding loss in spatial resolution at increased window lengths can be observed in these figures [18].

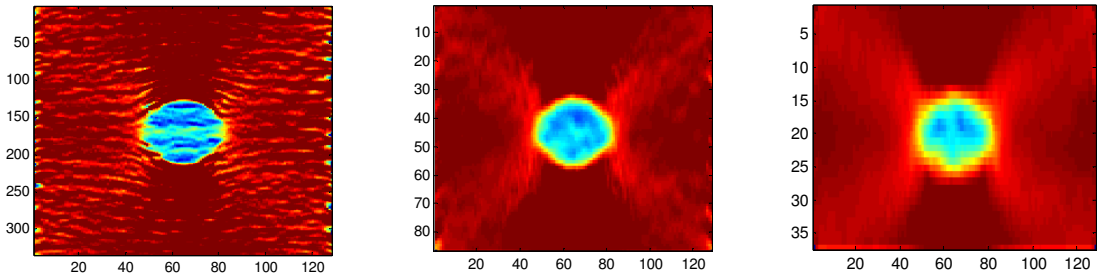

(a) (b) (c)

Fig. 13. Examples of elastograms obtained using GCC-FFT at different window lengths: (a) 0.5 mm (b) 2 mm (c) 4 mm.

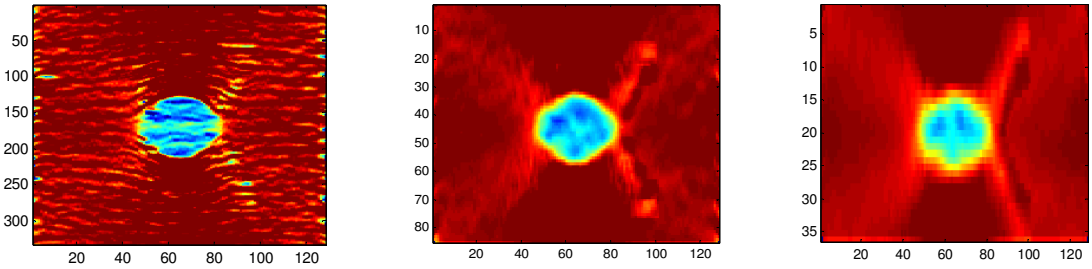

(a) (b) (c)

Fig. 14. Examples of elastograms obtained using GCC-PE at different window lengths: (a) 0.5 mm (b) 2 mm (c) 4 mm.

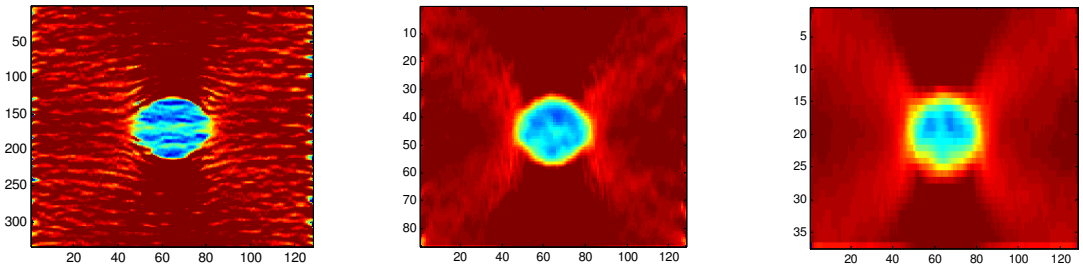

(a) (b) (c)

Fig. 15. Examples of elastograms obtained using GCC-FRFT at different window lengths: (a) 0.5 mm (b) 2 mm (c) 4 mm.

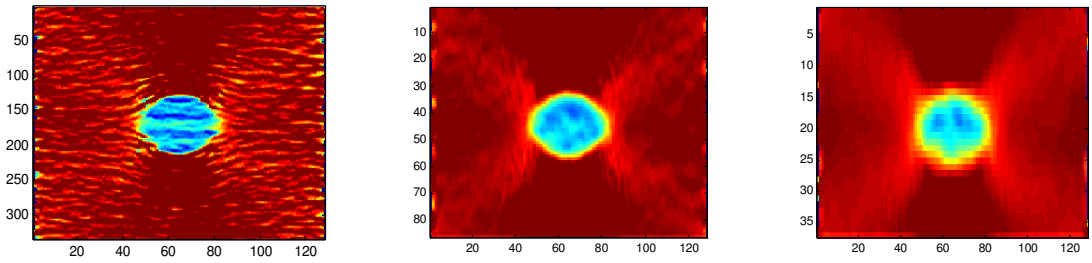

(a) (b) (c)

Fig. 16. Examples of elastograms obtained using SSD at different window lengths: (a) 0.5 mm (b) 2 mm (c) 4 mm.

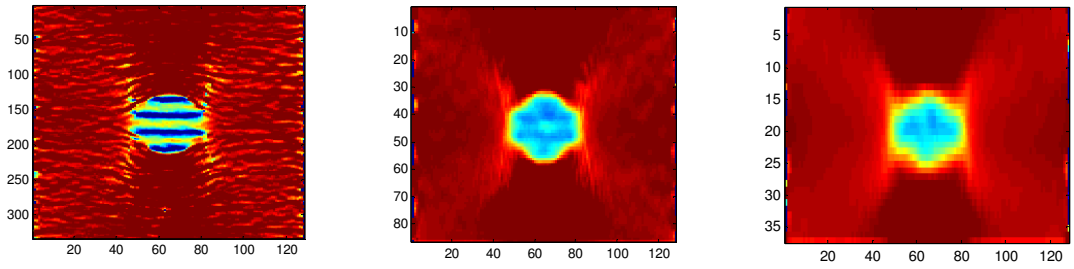

(a) (b) (c)

Fig. 17. Examples of elastograms obtained using SAD at different window lengths: (a) 0.5 mm (b) 2 mm (c) 4 mm.

F. Results- Image Quality Analysis

1. SNR_e

Fig 18 shows the strain filter curves corresponding to the different algorithms cross correlation based algorithms implemented in this study. Each point in the graph is an average over 50 independent realizations; the error bars represent the standard deviation. It can be seen from this graph that all GCC algorithms have similar performance with respect to SNR_e in the range of strains considered in this study. For very low strains, the GCC-FFT algorithm appears to outperform the other GCC methods.

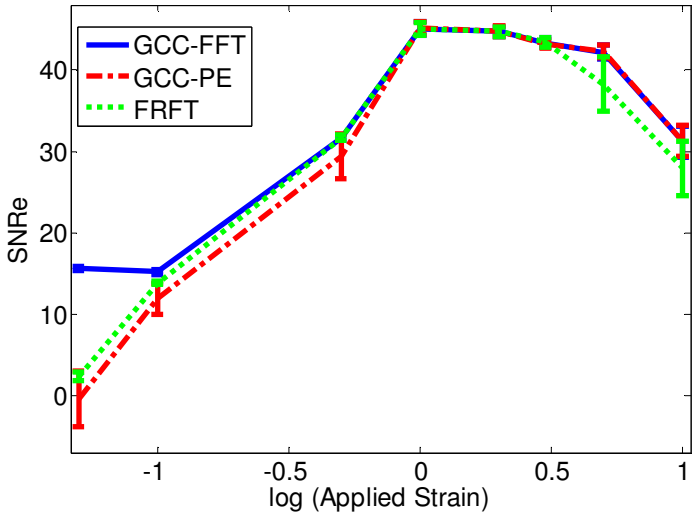

Fig. 18. Strain filters corresponding to the Generalized Cross Correlation methods implemented in this study.

Fig 19 shows simulated strain filter curves corresponding to the SAD and SSD algorithms implemented in this study. It can be seen from these graphs that the SSD method appears to outperform the SAD method for most values of applied strains.

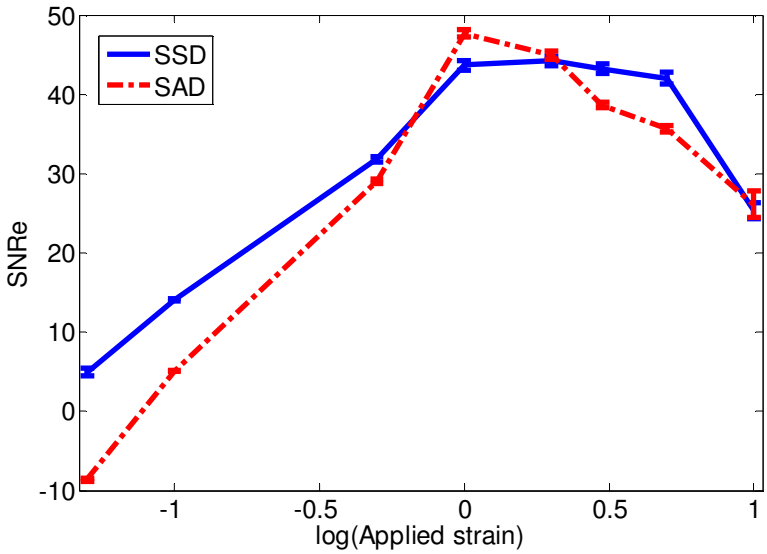

Fig. 19. Strain filters corresponding to the SSD and SAD methods implemented in this study.

Table I shows the values of SNR obtained for the various TDE algorithms for the range of applied strains considered in this study. From the SNR values, it can be seen that the images obtained using GCC-FFT and GCC-FRFT methods have higher values of SNR_e for most values of applied strains as compared to the other methods.

Table I. SNR_e values for the various algorithms for different values of applied strains.

Applied Strain %	GCC-FFT	GCC-PE	GCC-FRFT	SSD	SAD
0.05	15.6848	-0.3713	2.3775	4.9217	-8.6363
0.1	15.2313	11.9307	13.83	14.0346	5.0704
0.5	31.6763	29.4375	31.68	31.842	29.0279
1	45.1074	45.2014	45.1	43.6747	47.6906
2	44.7227	44.7659	44.72	44.22	44.9321
3	43.4051	43.1903	43.40	43.2186	38.6313
5	42.2105	42.286	38.22	42.0449	35.6311
10	31.2227	31.3055	27.92	25.3672	26.0959

Table II shows the results of the statistical analysis performed to test for the presence of statistically significant differences among the SNR_e measurements as obtained from the various TDE algorithms. In Table II, we indicate the values of strains for which the p-value computed on the SNR_e results of two different algorithms is less than 0.05, which would indicate a statistically significant difference between the two sets of results at a 95% confidence level. This table confirms that the findings reported in Table 1 are statistically significant.

Table II. Strains for which the p-value between sets of measurements of SNR_e obtained using two algorithms were found < 0.05.

	GCC-FFT	GCC-PE	GCC-FRFT	SSD	SAD
GCC-FFT	-	0.05%, 0.1%, 0.5%	0.05%, 0.1%, 0.5%, 10%	All applied strains, except 3% and 5%	All applied strains, except 2%
GCC-PE	0.05%, 0.1%, 0.5%	-	All applied strains, except 1%, 3% and 5%	All applied strains, except 3% and 5%	All applied strains, except 3% and 5%
GCC-FRFT	0.05%, 0.1%, 0.5%, 10%	All applied strains, except 1%, 3% and 5%	-	All applied strains, except 0.5% and 3%	All applied strains, except 2% and 10%
SSD	All applied strains, except 3% and 5%	All applied strains, except 3% and 5%	All applied strains, except 0.5% and 3%	-	All applied strains
SAD	All applied strains, except 2%	All applied strains, except 0.5% and 2%	All applied strains, except 2% and 10%	All applied strains	-

2. CNR_e

Fig 20 shows the CNR_e as a function of strain for the different GCC algorithms implemented in this study. Each point in the graph is an average over 50 independent realizations; the error bars represent the standard deviation. It can be inferred from these curves that the performances of GCC- FFT method and GCC-FRFT are similar for most values of applied strains except at very low (at 0.01 % GCC-FFT performs better) and

very high values of strains (at 10 % GCC-FRFT performs better). It can also be noted that the GCC-FFT method outperforms the GCC-PE at all the applied strains.

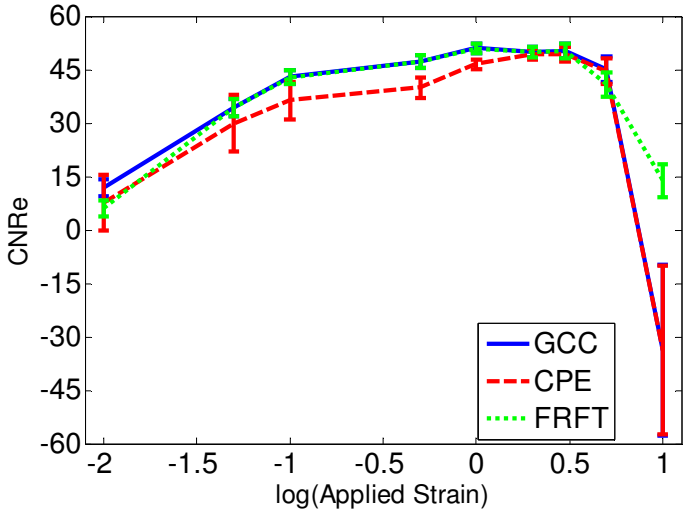

Fig. 20. CNR_e as a function of strain for Generalized cross correlation (GCC) methods.

Fig 21 shows the CNR_e as a function of strain for the SSD and SAD algorithms implemented in this study.

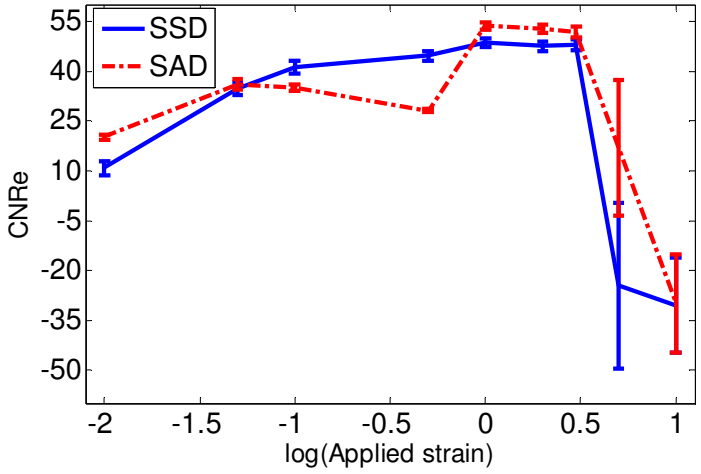

Fig. 21. CNR_e as a function of strain for the SSD and SAD methods.

Table III shows the values of CNR_e obtained for various algorithms at different values of applied strains.

Table III. CNR_e values for the various algorithms for different values of applied strains.

Applied Strain (%)	GCC-FFT	GCC-PE	GCC-FRFT	SSD	SAD
0.01	11.8507	7.685	6.06	10.8656	20.16
0.05	34.3976	29.9286	34.32	34.7383	36.0595
0.1	42.9188	36.304	42.89	41.0946	35.1714
0.5	47.1768	40.0102	47.18	44.6693	28.1369
1	51.0146	46.5297	50.98	48.5919	53.6217
2	49.9445	49.3774	49.925	47.5814	52.64
3	50.2566	49.3224	50.27	48.0536	51.7895
5	45.0803	44.6614	40.9	-24.5763	16.8963
10	-33.7706	-33.7584	13.92	-30.4459	-29.8481

The results reported in Table III suggest that the GCC algorithms outperform SSD and SAD methods, especially at higher values of applied strains (this difference is also visible from the strain elastograms shown earlier).

These observations were verified statistically by computing the p-values, which are reported in Table IV. In Table IV, we indicate the values of strains for which the p-value computed on the CNR_e results of two different algorithms is less than 0.05, which would indicate a statistically significant difference between the two sets of results at a 95% confidence level. From Table IV, GCC-FFT and GCC-FRFT indicate that they are statistically similar for most values of the applied strains except at very low (0.1 %) and high values (10 %) of strains.

Table IV. Strains for which the p-value between sets of measurements of CNR_e obtained using two algorithms were found < 0.05.

	GCC-FFT	GCC-PE	GCC-FRFT	SSD	SAD
GCC-FFT	-	All applied strains, except 2% 5% and 10%	0.1% and 10%	All applied strains, except 0.05% and 10%	All applied strains, except 5% and 10%
GCC-PE	All applied strains, except 2% 5% and 10%	-	All applied strains, except 0.01% and 2%	All applied strains, except 0.01% and 10%	All applied strains, except 0.1% and 10%
GCC-FRFT	0.1% and 10%	All applied strains, except 0.01% and 2%	-	All applied strains, except 0.05%	All applied strains
SSD	All applied strains, except 0.05% and 10%	All applied strains, except 0.01% and 10%	All applied strains, except 0.05%	-	All applied strains, except 10%
SAD	All applied strains, except 5% and 10%	All applied strains, except 0.1% and 10%	All applied strains	All applied strains, except 10%	-

3. Dynamic Range

Table V shows the values of dynamic range obtained for the various algorithms considered in this study. As we can see from the table, the values of dynamic range of GCC methods and SSD are fairly close to each other, while SAD appears to suffer of a lower dynamic range than the other methods.

Table V. Dynamic range estimated for the various TDE algorithms implemented in this study.

TDE Algorithm	Uniform case(dB)	Inclusion case(dB)
GCC-FFT	29.13	43.83
GCC-PE	27.92	38.19
FRFT	26.36	44.51
SSD	25.8	39.45
SAD	23.34	18.38

Table VI reports the results of the statistical analysis performed on the dynamic range results. In Table VI, the actual p-values found out using t-testing is reported.

Table VI. p-values obtained for dynamic range measurements.

	GCC-FFT	GCC-PE	GCC-FRFT	SSD	SAD
GCC-FFT	-	0.002	0	0	0
GCC-PE	0.002	-	0.0001	0	0
GCC-FRFT	0	0.0001	-	0.013	0
SSD	0	0	0.013	-	0
SAD	0	0	0.013	0	-

From the Tables V and VI, it can be seen that the dynamic range associated with GCC methods is statistically significantly higher than that of SSD and SAD methods.

4. Sensitivity

Table VII shows the results of the sensitivity study performed on the algorithms implemented in this study.

Table VII. Sensitivity of the various algorithms.

TDE Algorithm	Uniform case(%)	Inclusion case(%)
GCC-FFT	0.4248	0.037
GCC-PE	0.496	0.0477
FRFT	0.43	0.039
SSD	0.4236	0.0367
SAD	0.518	0.52

Overall, the sensitivity values of GCC-FFT and SSD algorithms were found to be better than the other algorithms. From the p-values reported in Table VIII, it can be seen that the sensitivity of GCC-FFT and SSD algorithms is statistically significantly higher than the sensitivity of the other algorithms.

Table VIII. p-values obtained for sensitivity measurements.

	GCC-FFT	GCC-PE	GCC-FRFT	SSD	SAD
GCC-FFT	-	0	0.03	0.63	0
GCC-PE	0	-	0	0	0.01
GCC-FRFT	0.03	0	-	0.007	0
SSD	0.63	0	0.007	-	0
SAD	0	0.01	0	0	-

5. Computational Time

Table IX shows the results of the computational time study performed on the algorithms implemented in this study.

Table IX. Computational time per pixel [s] for the various algorithms implemented in this study.

Algorithm	Time to calculate displacement for one pixel (sec)
GCC-FFT	4.4497e-004 ± 1.9538e-005
GCC-PE	1.1649e-004 ± 4.2218e-006
GCC-FRFT	0.0532 ± 0.0039
SSD	0.0033 ± 1.6258e-004
SAD	0.0035 ± 2.6729e-004

In our implementations of the various TDE algorithms, the GCC-PE method is the fastest of all methods, followed by the GCC-FFT method. The GCC-FRFT, SSD and SAD methods, instead, appear to be significantly slower. These results are expected because, as previously explained, the PE method uses prior knowledge to reduce computational time.

G. Experimental Results

Figures 22 and 23 show experimental results obtained from a phantom containing a cylindrical inclusion. These results were used just as a proof of principle of the applicability of the various algorithms to real data. These results were not used for statistical analysis.

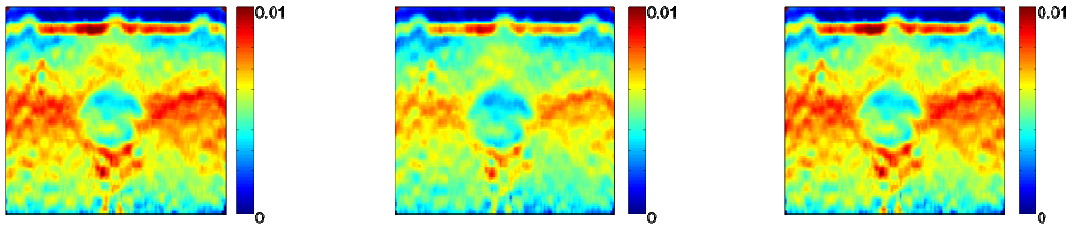

GCC-FFT GCC-PE GCC-FRFT

Fig. 22. Experimental results obtained using the GCC methods.

SSD SAD

Fig. 23. Experimental results obtained using the SSD and SAD methods.

H. Summary

In this chapter, we reported the technical details relative to the various TDE algorithms implemented in this study. We also reported a statistical analysis on the performance of these algorithms using simulations. These results suggest that the GCC methods outperform SSD and SAD methods for all image quality factors analyzed for this study.

CHAPTER V

CONCLUSIONS AND FUTURE WORK

A. Conclusions

In this thesis, a comparative study of various time delay estimation algorithms for elastography was performed. The TDE methods considered included: methods based on generalized cross correlation, methods based on sum of squared differences, and methods based on sum of absolute differences. Within the generalized cross correlation methods, we considered: FFT-based method, correlation with prior estimates, and Fractional Fourier Transform method. The performance of the various TDE techniques was statistically analyzed based on various performance indicators. Based on the results of the analysis performed in this study, performance indicators of correlation-based algorithms are statistically significantly higher than performance indicators of SSD and SAD algorithms both at low strains and high strains. This would indicate that correlation-based algorithms are more sensitive and more robust than SSD and SAD methods.

Within the class of GCC methods, the FFT-based method appears to outperform the other GCC methods considered for this study. Though correlation with prior estimates outperforms other algorithms in terms of speed of computation, the quality of the image produced appears to be compromised when compared to the FFT generalized cross correlation method.

The Fractional Fourier Transform based algorithm theoretically finds normalized correlation coefficient that are greater than or equal to those obtained from FFT generalized cross correlation method. Its performance in terms of CNR is better than GCC-FFT at high values of strains but at applied strains its performance is statistically comparable with the performance of GCC-FFT, with the disadvantage of being significantly slower.

B. Future Work

The algorithms considered in this study were all based on cost functions. In the future, the study could be extended to algorithms based on individual sample tracking [20] or zero-crossing methods. .

Though all the algorithms that were implemented in this study are capable of obtaining both axial and lateral displacement and strain estimations, their performances were investigated only for the axial case. However, an analysis of the performance of these algorithms for the lateral case is currently undergoing.

Finally, the simple simulation models used in this work are based on simplistic noise conditions and, thus, represent an optimistic scenario with respect to real data. In this study, we reported a proof-of-principle of the applicability of these algorithms to experimental real data, but no statistical analysis could be performed on these data. In the future, it will be very important to extend this study to real data and test the performance of these algorithms in situations of clinical interest.

REFERENCES

[1] J. Ophir, I. Cespedes, B. Garra, H. Ponnekanti, Y. Huang, and N. Maklad, "Elastography: Ultrasonic imaging of tissue strain and elastic modulus in vivo," *European Journal of Ultrasound,* vol. 3, pp. 49-70, 1996.

[2] J. Ophir, K. Alam K, B. Garra, F. Kallel, E. E. Konofagou, T. A. Krouskop, and T. Varghese, "Elastography: Ultrasonic estimation and imaging of the elastic properties of tissues," *Proceedings of the Institution of Mechanical Engineers*, pp. 1-31, 1999.

[3] T.A. Krouskop , T.M. Wheeler, F. Kallel, B.S. Garra, and T. Hall, "Elastic moduli of breast and prostate tissues under compression," *Ultrasonic Imaging*, vol. 20, pp. 260-274, 1998.

[4] E. I. Cespedes, "Elastography: Imaging of biological tissue elasticity," Ph.D. dissertation, University of Houston, Houston, TX, 1993.

[5] J. Ophir, I. Cespedes, H. Ponnekanti, Y. Yazdi, and X. Li, "Elastography: A method for imaging elasticity of biological tissues," *Ultrasonic Imaging*, vol. 13, pp. 111-134, 1991.

[6] F. Viola and W.F. Walker**,** "A comparison of time delay estimators for medical ultrasound," *IEEE Transactions on Ultrasonics, Ferroelectrics and Frequency Control*, vol. 50, pp. 393-401, Apr 2003.

[7] T. Varghese and J. Ophir, "Enhancement of echo-signal correlation in elastography using temporal stretching," *IEEE Transactions on Ultrasonics, Ferroelectrics, and*

Frequency Control, vol. 44, no. 1, Jan 1997.

[8] S. Srinivasan, R. Righetti, and J. Ophir, "Tradeoffs between signal to noise ratio and axial resolution in ultrasound elastography," *Ultrasound in Med. & Biol*., vol. 29, no. 6, pp. 847–866, 2003.

[9] Stanford University Center for Computer Research in Music and Acoustics, "Matlab for Parabolic Peak Interpolation," https://ccrma.stanford.edu/~jos/sasp/M-atlab _Parabolic_Peak_Interpolation.html, accessed in Jan 2010.

[10] S. Srinivasan, J. Ophir, and S.K. Alam, "Elastographic imaging using staggered strain estimates," *Ultrasonic Imaging*, vol. 24, pp. 229- 245, 2002.

[11] F. Kallel and J. Ophir, "A least squares estimator for elastograph, *Ultrasonic Imaging*," vol. 19, no. 3, pp. 195-208, 1997.

[12] J. Bendat, and A. Piersol, *Random Data: Analysis and Measurement Procedure*, John Wiley and Sons, New York, 1986.

[13] T. Varghese and J. Ophir, "Performance optimization in elastography: Multi-compression with temporal stretching," *Ultrasonic Imaging*, vol. 18, pp. 193-214, 1996.

[14] R. Zahiri-Azar and S. Salcudean, "Motion estimation in ultrasound images using time domain cross correlation with prior estimates," *IEEE Transactions on Biomedical Imaging*, vol. 53, no. 10, pp. 1990-2000, Oct 2006.

[15] Wikipedia, "Fractional Fourier Transform," http://en.wikipedia.org/wiki/Fraction-al_Fourier_Transform, accessed in May 2010.

[16] M.A. Kutay, H.M. Ozaktas, O. Arikan, and L. Onural, "Optimal filtering in

fractional Fourier Domains," *IEEE Transactions on Signal Processing*, vol. 45, no. 5, pp. 1129 – 1143, May 1997.

[17] Y. Bitran, Z. Zalevsky, D. Mendlovic, and R.G. Dorsch, "Fractional correlation operation: performance analysis," *Applied Optics*, vol. 35, pp. 297-303, 1996.

[18] R. Righetti, J. Ophir, and P. Ktonas, "Axial resolution in elastography," *Ultrasound in Med. & Biol.*, vol. 28, no. 1, pp. 101-113, 2002.

[19] T. Varghese and J. Ophir, "A theoretical framework for performance characterization of elastography: The strain filter," *IEEE Transactions on Ultrasonics, Ferroelectrics, and Frequency Control*, vol. 44, pp. 164-172, no. 1, Jan 1997.

[20] R. Zahiri-Azar and S. Salcudean, "Time delay estimation in ultrasound echo signals using individual sample tracking," *IEEE Transactions on Ultrasonics, Ferroelectrics, and Frequency Control*, vol. 55, no. 12, Dec 2008.

VITA

Name: Srinath Sambasubramanian

Address: Department of Electrical and Computer Engineering,
Texas A&M University,
214 Zachry Engineering Center,
TAMU 3128,
College Station, Texas 77843-3128

Education: B.Tech, Instrumentation and Control Engineering
National Institute of Technology, Trichy, 2005

M.S., Electrical Engineering, Texas A&M University, 2010